THE JOURNAL OF NAVIGATION (2019), 1–11.
doi:0000000000

Greedy Algorithm based Integrity Monitoring for Visual Navigation

Chen Zhu[1] and Mehmet Berk Takim[2] and Michael Meurer[1,2]

[1]*German Aerospace Center (DLR), Institute of Communications and Navigation, Oberpfaffenhofen, Germany*
[2]*RWTH Aachen University, Chair of Navigation, Aachen, Germany*
(E-mail: Chen.Zhu@dlr.de)

Camera-based visual navigation techniques have several advantages to provide positioning and navigation solutions in environments like urban areas, and appropriate integrity monitoring is required to apply the techniques to safety-critical applications. For satellite navigation, as prior fault probabilities of satellites are low, three or more simultaneous and independent faults constitute an insignificant part of the integrity risk budget. Consequently, Receiver Autonomous Integrity Monitoring (RAIM) techniques can afford exhaustive search over all hypotheses corresponding to the limited number of fault modes for fault detection and elimination. However, in visual navigation, both the fault probability and the number of measurements are usually much larger than in satellite navigation, so an exhaustive search over all the fault modes becomes computationally infeasible, if a similar level of integrity performance is required. To cope with the specific challenge for visual navigation, we propose a greedy algorithm based integrity monitoring method with polynomial complexity with respect to the maximum number of faults to be monitored. The integrity risk analysis for the proposed method is provided. The proposed method is compared with the state-of-the-art method in simulations and significantly outperforms it in runtime.

KEYWORDS

visual positioning. integrity monitoring. navigation safety. solution separation.

1. INTRODUCTION. Positioning and navigation services have become an essential part of our daily life. As new applications emerge, the requirements on navigation systems is also increasingly stringent. Safety critical applications like autonomous driving and urban air mobility require not only high-accuracy but also high- integrity solutions in challenging environments such as deep urban areas. As a widely used core technique for positioning, Global Navigation Satellite Systems (GNSS) faces performance degeneration in such environments due to shadowing by tall buildings and strong multipath signals. In order to fulfill the performance requirements, a multi-sensor solution is necessary. Visual navigation using cameras is a valuable component of the solution in such scenarios due to its advantages in precision, costs, huge amount to information, and visualization capability, etc. However, the integrity monitoring of visual positioning methods is a challenging topic and requires innovative approaches to cope with specific new problems (Zhu(2020).

The integrity monitoring methods for GNSS have been developed in the past decades, and are playing an important role in safety critical applications like civil aviation. The Receiver Autonomous Integrity Monitoring (RAIM) techniques provide the possibility to automatically detect and exclude faulty measurements with large biases, and are capable of calculating a protection level to monitor the integrity of the solution. Residual based statistic tests are applied in RAIM (Brown(1994). The residual based approach has been extended to multiple fault cases by Angus in (Angus(2006). As the technique develops, advanced RAIM (ARAIM) methods (Blanch(2015) are proposed to satisfy the more demanding requirements. Multiple hypothesis solution separation (MHSS) (Blanch(2007) method is used in ARAIM, and becomes a state-of-the-art approach for fault detection and integrity monitoring. The method decompose the possible combinations of faulty measurements into different hypotheses, and searches all the possible fault modes to isolate faulty measurements from the bias-free ones. As the prior failure rate and the total number of measurements are relatively low for GNSS, it is feasible to exhaustively loop over all the fault modes. However, in visual navigation, the prior fault probability of measurements is much larger. An exhaustive search over all the possible fault modes becomes infeasible from computational complexity point of view, since the complexity grows exponentially with the maximum number of faults to be monitored. As a possible solution, an innovative method is proposed in this work based on the philosophy of greedy algorithm, in order to detect multiple biased measurements in feasible time even if the potential number for faults is large.

The structure of this paper is as following: the measurement model of camera based positioning is first introduced, followed by the discussion on the complexity problem in applying the state-of-the-art multiple hypotheses solution separation methods to visual positioning. Then a greedy solution separation algorithm is proposed to cope with the aforementioned problem. The integrity analysis for the new algorithm is provided in the following section. Then, the simulation results are shown to demonstrate the algorithm performance. In the end, the conclusions are drawn.

2. MEASUREMENT MODEL OF CAMERA-BASED POSITIONING.

In the remainder of this paper, a superscript with parentheses $^{(\cdot)}$ is used to denote the reference frame in which the vector is represented. Vectors and matrices are denoted with bold symbols while scalars are not. Vectors such as $\vec{\mathbf{p}}_m^{(W)} \in \mathbb{R}^3$ with geometric meanings are written with an arrow. The homogeneous coordinates in the extended Euclidean plane are written as $\tilde{\mathbf{u}} \in \mathbb{P}^2$. $[\mathbf{A};\mathbf{B}]$ denotes vertical concatenation of two matrices.

In this work, a state-of-the-art pinhole model with corrected radial lens distortion is used as the sensor model of the camera. Fig. 1 illustrates the system model of a pinhole camera.

The projection of a point with coordinates $\vec{\mathbf{p}}_m^{(W)} \in \mathbb{R}^3$ to the camera is described as

$$\tilde{\mathbf{u}}_m = \mathbf{K}\mathbf{R}_{(C\to W)}^T(\vec{\mathbf{p}}_m^{(W)} - \vec{\mathbf{p}}_C^{(W)}), \tag{1}$$

where $\vec{\mathbf{p}}_C^{(W)}$ is the camera position in a global reference frame (W), and $\mathbf{R}_{(C\to W)} \in \mathbf{SO}(3)$ is the rotation matrix between the camera body frame (C) and frame (W). The matrix $\mathbf{K}$ is called camera intrinsic matrix, the parameters of which are only dependent on the camera and the lens. $\tilde{\mathbf{u}}_m = d[u_x, u_y, 1]^T$ is the location of the point m in the image plane in homogeneous coordinates, where d is the depth of the point, i.e., the distance of the point

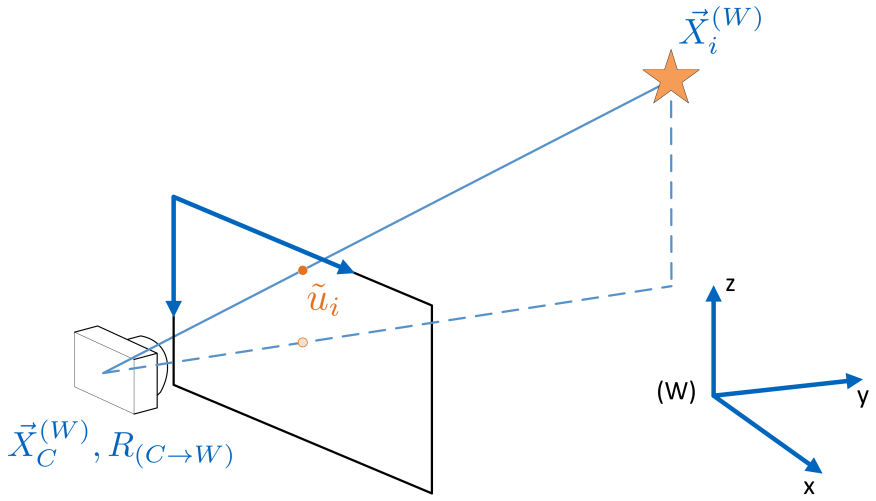

Figure 1.: System model of a pinhole camera

to the image plane. The depth can be expressed as

$$d = [0,0,1]\mathbf{R}_{(C\to W)}^{T}(\vec{\mathbf{p}}_m^{(W)} - \vec{\mathbf{p}}_C^{(W)}). \tag{2}$$

In Euclidean space, the 2D coordinates of a projected point in the image plane is related to the camera pose and the 3D location of the feature point as described in the following equation

$$\mathbf{u}_m = \begin{bmatrix} u_x \\ u_y \end{bmatrix} = \frac{1}{d}\begin{bmatrix} 1 & 0 & 0 \\ 0 & 1 & 0 \end{bmatrix}\tilde{\mathbf{u}}_m. \tag{3}$$

We parameterize the camera attitude using Rodrigues parameters $\mathbf{r} = [r_1, r_2, r_3]^T = \theta\boldsymbol{\eta}$, which can be related to the rotation matrix by Rodrigues rotation formula as (Shuster(1993)

$$\mathbf{R}_{(C\to W)} = \mathbf{I}_3\cos(\theta) + \lfloor\boldsymbol{\eta}\rfloor_\times \sin(\theta) + (1-\cos(\theta))\boldsymbol{\eta}\boldsymbol{\eta}^T, \tag{4}$$

where $\mathbf{I}_3$ is a 3-dimensional identity matrix, and $\lfloor\boldsymbol{\eta}\rfloor_\times$ is the skew symmetric matrix using the normalized unit vector $\boldsymbol{\eta} = \mathbf{r}/\|\mathbf{r}\| \in \mathbb{R}^3$ as none-zero entries. The operator $\lfloor\cdot\rfloor_\times$ is defined as

$$\lfloor\boldsymbol{\eta}\rfloor_\times = \begin{bmatrix} 0 & -\eta_3 & \eta_2 \\ \eta_3 & 0 & -\eta_1 \\ -\eta_2 & \eta_1 & 0 \end{bmatrix}. \tag{5}$$

It should be mentioned that the three Roderigues parameters are corresponding to the coefficients of the Lie algebra of the $\mathbf{SO}(3)$ group (Murray(2017). The rotation can be equivalently represented as

$$\mathbf{R}_{(C\to W)} = \exp(\lfloor\mathbf{r}\rfloor_\times), \tag{6}$$

where $\exp(\cdot)$ is matrix exponential operator. Such minimal parameterization of attitude is convenient for operations on manifold. It is mathematically elegant, and is capable of avoiding the Gimbal lock problem of Euler angle parameterization (Shuster(1993).

Consequently, we can parameterize the camera pose with a 6 degrees-of-freedom (DoF) vector

$$\mathbf{x} = \begin{bmatrix} \vec{\mathbf{p}}_C^{(W)} \\ \mathbf{r} \end{bmatrix} \in \mathbb{R}^6. \tag{7}$$

In order to simplify the notation, a function $\pi_m(\cdot) : \mathbb{R}^6 \to \mathbb{R}^2$ is defined to project the 3D point $\vec{\mathbf{p}}_m^{(W)}$ to the 2D coordinates in the image plane of a camera with 6DoF pose parameterized as $\mathbf{x}$. The projection can be explicitly expressed as

$$\mathbf{u}_m = \pi_m(\mathbf{x}) = \frac{\begin{bmatrix} 1 & 0 & 0 \\ 0 & 1 & 0 \end{bmatrix} \mathbf{K}\mathbf{R}_{(C\to W)}^T(\vec{\mathbf{p}}_m^{(W)} - \vec{\mathbf{p}}_C^{(W)})}{\begin{bmatrix} 0 & 0 & 1 \end{bmatrix} \mathbf{K}\mathbf{R}_{(C\to W)}^T(\vec{\mathbf{p}}_m^{(W)} - \vec{\mathbf{p}}_C^{(W)})}. \tag{8}$$

Consequently, for a feature point m extracted from the measurement image, the noisy measurement equation can be expressed as

$$\mathbf{z}_m = \mathbf{u}_m + \mathbf{n}_m + \mathbf{b}_m = \pi_m(\mathbf{x}) + \mathbf{n}_m + \mathbf{b}_m, \tag{9}$$

where $\mathbf{n}_m$ is zero-mean Gaussian noise with covariance matrix $\mathbf{\Sigma}_{n_m}$, which can be conservatively modelled using the method in (Zhu(2019), and $\mathbf{b}_m$ is the systematic bias in the feature location that can be caused by various effects such as feature detection bias. If the measurement j is unbiased, $\mathbf{b}_m = 0$.

Given N_p feature points in the map (requiring $N_p \geq 4$ in general), the position and orientation of the camera can be estimated using corresponding 2D measurements $\{m = 1, ..., N_p | z_m\}$ by iteratively solving the following nonlinear optimization problem

$$\hat{\mathbf{x}} = \arg\min_{\mathbf{x}} \|\mathbf{z} - \pi(\mathbf{x})\|^2_{\mathbf{\Sigma}_n^{-1}}, \tag{10}$$

where

$$\mathbf{z} = \begin{bmatrix} \mathbf{z}_1 \\ \vdots \\ \mathbf{z}_{N_p} \end{bmatrix}, \pi(\mathbf{x}) = \begin{bmatrix} \pi_1(\mathbf{x}) \\ \vdots \\ \pi_{N_p}(\mathbf{x}) \end{bmatrix}, \mathbf{n} = \begin{bmatrix} \mathbf{n}_1 \\ \vdots \\ \mathbf{n}_{N_p} \end{bmatrix}. \tag{11}$$

$\mathbf{\Sigma}_n$ is the covariance matrix of noise vector $\mathbf{n}$. The initial estimation for the linearization point can be obtained using the direct PnP methods such as in (Lepetit(2009). The optimization can be solved using iterative least-squares method by linearizing the measurement function $\pi(\mathbf{x})$ iteratively. The linearization error is a significant problem in visual navigation. However, it is not the main focus of this work, so it is assumed in the following sections that large linearization error can be monitored and the Jacobian matrix linearized at the converged solution $\mathbf{H}$ can approximate the local property of $\pi(\mathbf{x})$ well. Consequently, the pose is estimated from the linearized measurement equation which can be denoted as

$$\mathbf{z} = \mathbf{H}\mathbf{x} + \mathbf{n} + \mathbf{b}, \quad \text{where } \mathbf{z}, \mathbf{n}, \mathbf{b} \in \mathbb{R}^{2N_p}, \mathbf{H} \in \mathbb{R}^{2N_p \times 6}. \tag{12}$$

If a least-squares method is applied, the estimate is

$$\hat{\mathbf{x}} = (\mathbf{H}^\mathbf{T}\mathbf{W}\mathbf{H})^{-1}\mathbf{H}^\mathbf{T}\mathbf{W}\mathbf{z}, \quad \text{where } \mathbf{W} = \mathbf{\Sigma}_\mathbf{n}^{-1}, \tag{13}$$

with covariance $\mathbf{P} = (\mathbf{H}^\mathbf{T}\mathbf{W}\mathbf{H})^{-\mathbf{1}}$.

3. COMPLEXITY PROBLEM OF SOLUTION SEPARATION BASED INTEGRITY MONITORING. The form of measurement equation Eqn. (12) is the same as the general equation used for integrity analysis in satellite navigation, except that each sample point consists of two dimensional measurements. The estimation result $\hat{\mathbf{x}}$ is unbiased if and only if the bias vector $\mathbf{b} = \mathbf{0}$. The state-of-the-art multiple hypothesis solution separation (MHSS) (Blanch(2007) method can be applied to monitor the integrity of the result. It has been thoroughly analyzed by Joerger et al. in (Joerger(2012) (Joerger(2013) that compared with conventional residual based integrity monitoring methods (Angus(2006), solution separation approach has advantages in detection boundary and simplicity in implementation of fault exclusion and protection level calculation. In the multiple hypotheses statistical test, the null hypothesis $\mathscr{H}_0$ assumes that the measurements are bias-free. When there are N_f number of faulty measurements, i.e. feature point with large bias in this context, $\mathscr{C}_{N_p}^{N_f}$ fault hypotheses can be established corresponding to all the possibilities of the faulty measurements indices. For maximum monitored number of faulty measurements $N_{f,max}$, the total fault hypotheses number is

$$N_{\text{mode}} = \sum_{N_f=1}^{N_{f,max}} \mathscr{C}_{N_p}^{N_f} = \sum_{N_f=1}^{N_{f,max}} \frac{N_p!}{(N_p - N_f)!N_f!}. \tag{14}$$

One can index all the hypotheses into $\{i = 1,2,...,N_{\text{mode}} | \mathscr{H}_i\}$, and define a function $F(i) = N_f$ to denote the number of faults corresponding to the fault mode i. For each fault mode, a fault-tolerant subset of measurements can be constructed by excluding the hypothetically biased measurements conditioned on $\mathscr{H}_i\}$. Denoting the i-th fault-tolerant subset's measurements and geometric matrix as $\mathbf{z}_i$ and $\mathbf{H}_i$ respectively, a fault-tolerant estimate under hypothesis $\mathscr{H}_i\}$ can be obtained as

$$\hat{\mathbf{x}}_i = (\mathbf{H}_i^T \mathbf{W}_i \mathbf{H}_i)^{-1} \mathbf{H}_i^T \mathbf{W}_i \mathbf{z}_i, \quad \text{with covariance } \mathbf{P}_i = (\mathbf{H}_i^T \mathbf{W}_i \mathbf{H}_i)^{-1}. \tag{15}$$

The difference between the subset and the full-set estimation is

$$\boldsymbol{\Delta} = \hat{\mathbf{x}}_i - \hat{\mathbf{x}}, \quad \text{with covariance } \mathbf{P}_\Delta = \mathbf{P}_i - \mathbf{P}. \tag{16}$$

For k-th dimension of the pose (k=1,...,6), the solution separation test statistic can be calculated as

$$q_{i,k} = \boldsymbol{\alpha}_k^T |\boldsymbol{\Delta}|, \tag{17}$$

where $\boldsymbol{\alpha}_k \in \mathbb{R}^6$ is the selection vector with value 1 at the k-th element and 0 at all others. The test statistic can be applied in threshold tests to detect large biases in the measurements. The protection level is calculated only if the test has been passed for all the fault modes i and state dimensions k. Otherwise a fault exclusion process which loops over all the fault modes to find a fault-free subset is necessary to ensure the safety.

The maximum monitored fault number $N_{f,max}$ is calculated according to the integrity requirements and the a priori probability of faults. In satellite navigation, as prior fault probabilities of satellites are low, three or more simultaneous and independent faults constitute an insignificant part of the integrity risk budget. In addition, the total number of visible satellites is in most cases not more than 20-25, even in dual constellation case. Consequently, the total fault mode number N_{mode} is usually less than a few hundreds. Looping

over all the fault modes exhaustively is still computationally feasible. However, in visual navigation, the prior fault probability of each measurement is significantly higher due to the erroneous feature detection process. As a result, the maximum number of faults need to be monitored increases and the value of N_{mode} will increase exponentially. Table 1 shows the change of $N_{f,max}$ and N_{mode} as the integrity requirements vary. In the table, the number of features is set to 20 and the prior probability of a single feature point is set to 0.01, which is already a relatively optimistic assumption for visual navigation. It can be seen that in the least demanding case, the total fault mode number is already 1350. If the integrity requirement is 10^{-6}, an exhaustive search over all the 21699 fault modes becomes computationally infeasible for ordinary hardware. If the prior probability is assumed to be 0.1, at most 9 faults need to be monitored for 10^{-4} integrity requirement, and the total fault mode number would increase to as huge as 431909.

Table 1. Number of Faults to Monitor and Total Fault Modes for $N_p = 20, p_{prior} = 0.01$

IR_{max}	10^{-4}	10^{-5}	10^{-6}	10^{-7}
$N_{f,max}$	3	4	5	5
N_{mode}	1350	6195	21699	21699

Additionally, the total number of available feature points are also usually much larger. This problem can be mitigated by selecting only the best features. Nevertheless, the exponential explosion in complexity due to large number of faults to be monitored has limited the usage of the state-of-the-art MHSS based integrity monitoring algorithm in visual navigation for safety critical applications.

4. GREEDY SOLUTION SEPARATION ALGORITHM FOR FAST INTEGRITY MONITORING.

In order to solve the complexity problem, an innovative integrity monitoring method based on greedy algorithm is described in this section. Blanch et al. proposed a residual based greedy search method in (Blanch(2015)) for GNSS integrity monitoring. However, no detailed integrity analysis was provided in the paper. Compared with Blanch's approach, tests under single-fault hypotheses is applied in this algorithm in order to benefit from the advantages of solution separation methods, while keeping the computational complexity polynomial with respect to the maximum number of faults to be monitored. The flowchart of the proposed method, which is referred to as greedy solution separation algorithm, is shown in Fig. 2.

The integrity check starts at iteration index $t = 1$ with an initial estimation if the total number of feature points is larger than 4, i.e., there is redundant measurements to execute integrity check. Following the full-set estimation, a total number of $N_{p,t}$ single-fault hypotheses and the corresponding fault-tolerant subsets are established. For each hypothesis, a test statistic $q_{i,k}$ can be calculated as Eqn. (17) following the same procedure as the state-of-the-art MHSS method for each subset and each dimension of the states. A threshold test must be passed for all the test statistics, i.e. $q_{i,k} \leq T_{SS,i,k}, \forall i,k$. The search space of different subsets reduces to $N_{p,t}$ from much larger N_{mode}, at a cost that it is no longer guaranteed that a bias-free estimate $\hat{\mathbf{x}}_i$ exists under one of the hypotheses, because only single-fault cases are assumed. In order to still ensure sufficient level of safety, a residual-based test

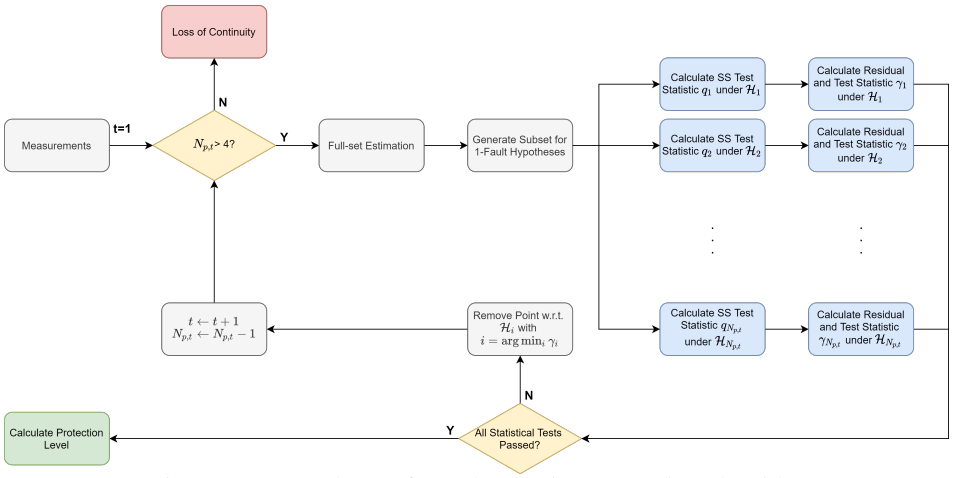

Figure 2.: Procedures of greedy solution separation algorithm

statistic γ_i is calculated as following for each single-fault-tolerant subset of measurements:

$$\gamma_i = \mathbf{z}_i^T(\mathbf{W}_i - \mathbf{W}_i\mathbf{H}_i(\mathbf{H}_i^T\mathbf{W}_i\mathbf{H}_i)^{-1}\mathbf{H}_i^T\mathbf{W}_i)\mathbf{z}_i. \tag{18}$$

γ_i is applied in a Chi-square test. The test threshold $T_{RB,i}$ can be calculated according to the continuity risk budget allocated to the test under hypothesis i. If the subset is fault-free, γ_i follows a central Chi-square distribution, otherwise it follows a non-central Chi-square distribution. If and only if all the tests are passed, i.e. $\gamma_i \leq T_{RB,i}, q_{i,k} \leq T_{SS,i,k}, \forall i,k$, the algorithm declares that no fault is detected and proceeds to protection level calculation. Otherwise, the measurements isolated under the hypothesis with maximum residual is removed, i.e. the feature point with respect to $\mathscr{H}_i\}$ with $i = \arg\max_i \gamma_i$ is removed. After the "worst" point is removed, the algorithm continues to the next iteration until all tests are passed in an iteration, or until insufficient points are remaining.

This proposed algorithm follows the philosophy of greedy algorithm that only a single locally-worst point is removed in each iteration. Consequently, the total number of statistical tests is proportional to $O(N_p N_{f,max})$. For exhaustive MHSS, the total number of tests is proportional to $O(N_{\text{mode}}) = O(N_p^{N_{f,max}})$. The search space decreases from exponential function to polynomial function of maximum monitored fault numbers.

5. INTEGRITY ANALYSIS OF THE GREEDY SS ALGORITHM.

In this section, the integrity of the greedy solution separation algorithm is analyzed. Hazardous misleading information events, denoted as HMI, happen if the algorithm does not detect any fault (the event demoted as ND), while the actual error in a certain dimension of the states has exceeded the alert limit l, i.e.

$$p_{\text{HMI}} = p(|\varepsilon| > l, \text{ND}) = \sum_{i=0}^{2^{N_p}-1} p(|\varepsilon| > l, \text{ND}|\mathscr{H}_i)p(\mathscr{H}_i). \tag{19}$$

The HMI probability are decomposed according to all the possible fault modes with $\mathscr{H}_0$ as the null hypothesis as no fault in the measurements. Without loss of generality, the

state dimension index k is waived for the purpose of conciseness. To fulfill the integrity requirements, it is essential that $p_{\text{HMI}} < \text{IR}_{max}$. The fault modes can be categorized by the number of faulty points as

$$\begin{aligned} p_{\text{HMI}} =& p(|\varepsilon| > l, \text{ND}|\mathscr{H}_0)p(\mathscr{H}_0) + \sum_{j\in J} p(|\varepsilon| > l, \text{ND}|\mathscr{H}_j)p(\mathscr{H}_j) \\ &+ \sum_{g\in G} p(|\varepsilon| > l, \text{ND}|\mathscr{H}_g)p(\mathscr{H}_g) + p(|\varepsilon| > l, \text{ND}|N_f > N_{f,max})p(N_f > N_{f,max}), \end{aligned} \tag{20}$$

where $J = \{j|F(j) = 1\}$ and $G = \{g|1 < F(g) \leq N_{f,max}\}$ denote the set of indices corresponding to hypotheses with single fault and monitored multiple faults respectively. The last term in Eqn. (20) can be upperbounded by $p(N_f > N_{f,max})$, which is lower than IR_{max}, so it can be subtracted from the total integrity budget and summation of the other three terms must be smaller than the remained integrity budget $\text{IR}_{max} - p(N_f > N_{f,max})$. The other terms' prior probability can also be easily calculated. The first conditional term in Eqn. (20) can be bounded by

$$p(|\varepsilon| > l, \text{ND}|\mathscr{H}_0) \leq p(|\varepsilon| > l|\mathscr{H}_0), \tag{21}$$

which can be easily calculated from the nominal error distribution.

As stated in the section 4, for the greedy solution separation algorithm, the no detection event is happening if and only if $\gamma_i \leq T_{RB,i}, q_i \leq T_{SS,i}, \forall i$. As a result, the second conditional term in Eqn. (20) can be bounded by

$$\begin{aligned} p(|\varepsilon| > l, \text{ND}|\mathscr{H}_j) &= p(|\varepsilon| > l, \gamma_i \leq T_{RB,i}, q_i \leq T_{SS,i}, \forall i|\mathscr{H}_j) \\ &\leq p(|\varepsilon| > l, \gamma_j \leq T_{RB,j}, q_j \leq T_{SS,j}|\mathscr{H}_j) \\ &\leq p(T_{SS,j} + |\varepsilon_j| > l, \gamma_j \leq T_{RB,j}|\mathscr{H}_j). \end{aligned} \tag{22}$$

The detailed derivation of Eqn. (22) can be found in (Joerger(2012). The terms can also be calculated from nominal error distribution since the fault-tolerant subset corresponding to $\mathscr{H}_j$ is fault-free.

For the multiple faults hypotheses, the conditional term can be bounded by

$$\begin{aligned} p(|\varepsilon| > l, \text{ND}|\mathscr{H}_g) &= p(|\varepsilon| > l, \gamma_i \leq T_{RB,i}, q_i \leq T_{SS,i}, \forall i|\mathscr{H}_g) \\ &\leq p(|\varepsilon| > l, \max \gamma_i \leq T_{RB,i}, \forall i|\mathscr{H}_j). \end{aligned} \tag{23}$$

The right hand side of the inequality can be calculated using the maximum slope for multiple faults residual based method in (Angus(2006).

As a result, an upperbound of all the terms can be calculated to compare with the integrity requirements for safety analysis. Equivalently, one can divide the total integrity budget that constrained by the requirement into each term of Eqn. (20) to calculate a protection level given the budget, and compare the most stringent protection level to a certain alert limit for integrity monitoring. The integrity of the solution can still be guaranteed using proposed greedy solution separation method, and the protection level calculation methods corresponding to the terms in Eqn. (20) are not much different from the state-of-the-art methods.

6. SIMULATION RESULTS. For all the simulations, simulated checkerboard images are used. The checkerboard size is set as 6×5 grid which corresponds to $N_p = 20$ number of inner corner 'X'-type features and each square has a side length of 40 mm. The top left square is set to black. Furthermore, the center of the checkerboard is assigned as the origin of the world coordinate frame. Intrinsic camera model parameters are selected to represent a simple camera with image dimensions of 1920×1200 pixels. Extrinsic camera model properties are set such that the camera faces the checkerboard directly at a distance of 1.25 meters. For the default bias profile, randomly selected 2 features ($N_f = 2$) are modeled to have a bias. Finally, nominal error model are derived for the simulated images following (Zhu(2019). The coefficients in the error model are assumed to be error-free in the simulations.

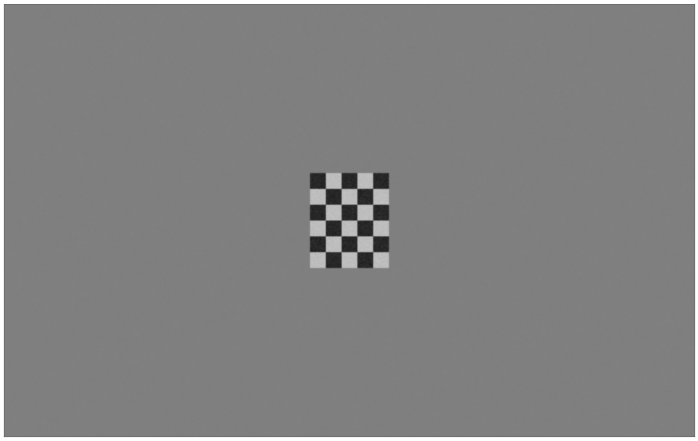

Figure 3.: An Example of a Simulated Image with Default Parameters

The runtime tests shown in this section are run on a laptop-computer (with Intel i7 CPU) using Matlab implementations for concept validation. It can be expected that a C/C++ implementation will significantly accelerate the program. With the proposed greedy solution separation algorithm (abbreviated as GSS in the following), very fast fault detection and exclusion can be performed. On top of the default 6×5 grid settings, additional checkerboard images with various dimensions are simulated to demonstrate the impact of total feature number on the runtime. The following grid sizes are tested in the simulation: $\{[5 \times 4], [5 \times 5], [6 \times 5], [6 \times 6], [7 \times 6]\}$ with 100 images for each set-up. The effect of the number of features on the simulation runtime is plotted in Fig. 4.

Fig. 5 compares the runtime for GSS and state-of-the-art solution separation method (Exhaustive SS) in the same scenario. As a reference, Random sample consensus (RANSAC) (Fischler(1981), another classic outlier rejection method which is widely used in visual navigation, is also included in the comparison. In this test, the default scenario with $N_p = 20$ is applied. It can be ssen that the proposed GSS method is significantly faster than the other two methods, esp. when the maximum number of faults $N_{f,max}$ is large. The runtime of the state-of-the-art exhaustive SS grows exponentially w.r.t. $N_{f,max}$, while the runtime of GSS method grows polynomially w.r.t. that.

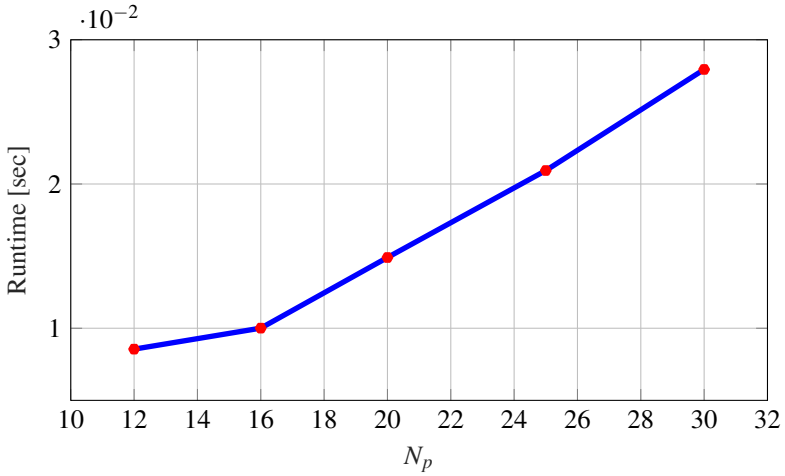

Figure 4.: GSS runtime vs. number of features N_p

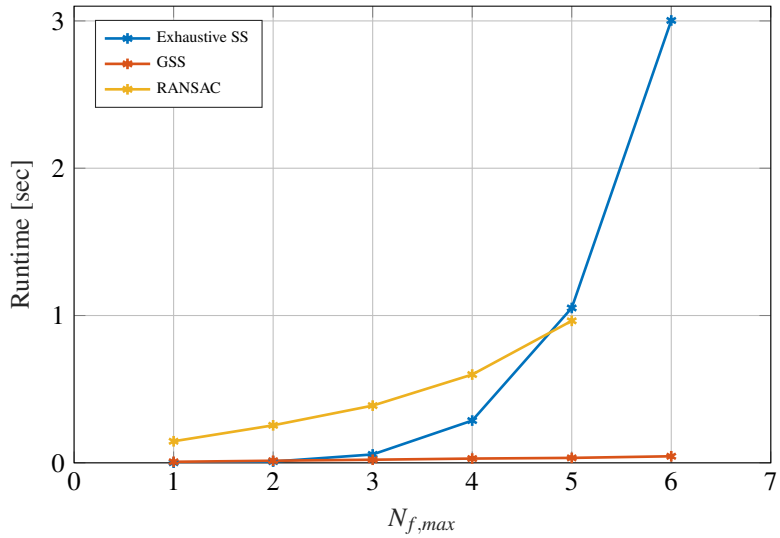

Figure 5.: Comparison of runtime of GSS, Exhaustive SS and RANSAC

7. CONCLUSION. A greedy solution separation is proposed in the work to solve the computational complexity problem in integrity monitoring of visual navigation. The method has polynomial complexity with respect to the maximum number of faults, and has significantly outperformed the state-of-the-art exhaustive-search MHSS method in runtime. The method can also potentially be applied to other applications with the same problem, e.g., for multi-constellation GNSS with very large number of visible satellites.

REFERENCES

M. D. Shuster: A Survey of attitude representations, vol. 1, no. 4, pp. 439–517, 1993.
R. M. Murray: A mathematical introduction to robotic manipulation, CRC press, 2017.

C. Zhu; C. Steinmetz; B. Belabbas; M. Meurer: Feature error model for integrity of pattern-based visual positioning, in *Proceedings of ION GNSS+ 2019, Miami, Florida*, 2019.

V. Lepetit; F. Moreno-Noguer; P. Fua: Epnp: An accurate o(n) solution to the pnp problem, *International Journal Of Computer Vision*, vol. 81, pp. 155–166, 2009.

J. Blanch; A. Ene; T. Walter; P. Enge: An optimized multiple hypothesis RAIM algorithm for vertical guidance, in *Proceedings of the 20th International Technical Meeting of the Satellite Division of The Institute of Navigation (ION GNSS 2007)*, 2007, pp. 2924–2933.

M. Joerger; F.-C. Chan; S. Langel; B. Pervan: Raim detector and estimator design to minimize the integrity risk, in *Proceedings of the 25th International Technical Meeting of the Satellite Division of the Institute of Navigation (ION GNSS 2012)*, 2012, pp. 2785–2807.

M. Joerger; S. Stevanovic; F.-C. Chan; S. Langel; B. Pervan: Integrity risk and continuity risk for fault detection and exclusion using solution separation araim, in *Proceedings of the 26th International Technical Meeting of the Satellite Division of The Institute of Navigation (ION GNSS+ 2013)*, 2013, pp. 2702–2722.

J. E. Angus: Raim with multiple faults, *Navigation*, vol. 53, no. 4, pp. 249–257, 2006.

Blanch, J.; Walter, T.; Enge, P. : Fast multiple fault exclusion with a large number of measurements. In *Proceedings of the 2015 International Technical Meeting of the Institute of Navigation*, pp. 696-701, 2015.

M. A. Fischler; R. C. Bolles: Random sample consensus: a paradigm for model fitting with applications to image analysis and automated cartography, *Communications of the ACM*, vol. 24, no. 6, pp. 381–395, 1981.

C. Zhu; M. Joerger; M. Meurer: Quantifying feature association error in camera-based positioning, in *2020 IEEE/ION Position, Location and Navigation Symposium (PLANS)*, pp. 967–972, 2020.

R. G. Brown: GPS RAIM: Calculation of thresholds and protection radius using chi-square methods. A geometric approach. Radio Technical Commission for Aeronautics, 1994.

J. Blanch; T. Walker; P. Enge; Y. Lee; B. Pervan; M. Rippl; A. Spletter; V. Kropp: Baseline advanced raim user algorithm and possible improvements, *IEEE Transactions on Aerospace and Electronic Systems*, vol. 51, no. 1, pp. 713–732, 2015.